Intersubband lifetimes in *p*-Si/SiGe terahertz quantum cascade heterostructures

R. W. Kelsall,[1,*] Z. Ikonic,[1] P. Murzyn,[2] C. R. Pidgeon,[2] P. J. Phillips,[2] D. Carder,[2] P. Harrison,[1] S. A. Lynch,[3] P. Townsend,[3] D. J. Paul,[3] S. L. Liew,[4] D. J. Norris,[4] and A. G. Cullis[4]

[1]*School of Electronic and Electrical Engineering, University of Leeds, Leeds, LS2 9JT, United Kingdom*

[2]*Department of Physics, Heriot-Watt University, Riccarton, Edinburgh, EH14 4AS, United Kingdom*

[3]*Cavendish Laboratory, University of Cambridge, Madingley Road, Cambridge, CB3 0HE, United Kingdom*

[4]*Department of Electronic & Electrical Engineering, University of Sheffield, Mappin Street, Sheffield, S1 3JD, United Kingdom*

(Received 2 September 2004; revised manuscript received 14 January 2005; published 28 March 2005)

Time-resolved studies of the dynamics of intersubband transitions are reported in three different strain symmetrized *p*-Si/SiGe multiple-quantum-well and quantum cascade structures in the far-infrared wavelength range (where the photon energy is less than the optical phonon energy), utilizing the FELIX free-electron laser. The calculated rates for optical and acoustic phonon scattering, alloy disorder scattering, and carrier-carrier scattering have been included in a self-consistent energy balance model of the transient far-infrared intersubband absorption, and show good agreement with our degenerate pump-probe spectroscopy measurements in which, after an initial rise time determined by the resolution of our measurement, we determine decay times ranging from ~2 to ~25 ps depending on the design of the structure. In all three samples the lifetimes for the transition from the first light hole subband to the first heavy hole subband are found to be approximately constant in the temperature range 4–100 K.

DOI: 10.1103/PhysRevB.71.115326 PACS number(s): 78.47.+p, 71.20.−b

I. INTRODUCTION

Following the considerable success of intersubband quantum cascade lasers (QCLs) based on InGaAs/InAlAs/InP and GaAs/AlGaAs heterostructures,[1] there has been much interest in developing a silicon-based QCL using the Si/SiGe system.[2] Since the lasers do not involve interband transitions, the indirect band gap of silicon and the SiGe alloys presents no hindrance to laser operation—the intersubband quantum cascade principle can be directly transferred to Si/SiGe heterostructures. Besides the obvious technological advantages of a silicon-based laser, in terms of low-cost processing and optoelectronic integration, the Si/SiGe materials system also offers various physical advantages for use in QCLs: the materials are nonpolar, so polar optical phonon scattering, which is the principal competing nonradiative process in III-V QCLs, is absent, and the energy of the dominant phonon mode in silicon is considerably higher than that in GaAs and InGaAs (64 meV compared to 36 meV), implying the existence of a larger frequency window in the terahertz range within which phonon scattering is suppressed.

The layer designs for III-V QCLs are generally very complex, with each period comprising an injector region (usually a chirped superlattice of up to ten quantum wells) and an active region comprising 2–4 quantum wells or, indeed, another chirped superlattice. This level of complexity, involving a large number of different layer thicknesses which must be grown to 0.1 nm precision, is very difficult to achieve in the strained Si/SiGe system. Therefore we have investigated a series of prototype cascade or "quantum staircase" structures based on a simple superlattice design. Our work to date has focused on *p*-type Si/SiGe heterostructures, which provide a large valence band offset and are of potential interest as surface-emitting QCLs, since the light to heavy hole transitions couple to surface-normal TE modes, without the need for any surface grating.[3] Our structures are also designed for emission in the far-infrared (FIR) or terahertz frequency range, for which QCLs have recently been shown to be one of the most promising solid-state sources.[4,5] Population inversion in the quantum staircase structures may be attained by engineering the relative subband lifetimes for interwell and intrawell transitions by adjustment of the well and barrier thicknesses and alloy compositions. However, even in these relatively simple layer designs, the band structure and intersubband transition rates are not straightforward to predict, and therefore direct measurement of intersubband lifetimes, as reported here, is important to characterize the performance of trial structures and to validate theoretical models which can then be used for the design of laser structures.

In previous work[6] we reported time-resolved far-infrared spectroscopy of intersubband transitions in *p*-Si/SiGe multiple-quantum-well structures, using the FELIX free-electron laser. In the following sections, we compare these results with pump-probe spectroscopy on two *p*-Si/SiGe quantum cascade samples. The transitions of interest are those between the first light hole (LH1) and first heavy hole (HH1) subbands, and in all three cases the LH1-HH1 energy gap at the zone center is less than the smallest optical phonon energy in the alloyed quantum well layers (the Ge-Ge mode phonon energy of 37 meV). Following description of the experimental configuration and results, we describe our theoretical model of the absorption recovery—which involves use of a self-consistent energy balance method and includes a six-band anisotropic $\mathbf{k}\cdot\mathbf{p}$ band structure, and phonon, alloy disorder, and carrier-carrier scattering processes—and explain how the experimental and theoretical data can be interpreted in order to develop an understanding of the intersubband physics of the *p*-Si/SiGe system.

 ©2005 The American Physical Society

II. EXPERIMENTAL DETAILS

One of the key features of QCLs is that a large number of periods (typically of the order of 100) are used to magnify the available gain. This approach is feasible in the strained Si/SiGe materials system only if the heterostructures are strain symmetrized. All our heterostructures are grown on a SiGe relaxed buffer or virtual substrate, which comprises a 3 μm linearly graded $Si_{1-x}Ge_x$ region, followed by 1 μm of SiGe at the end-point composition. The well and barrier thicknesses are then calculated, according to their respective Ge compositions, to ensure that the adjacent layers contain equal and opposite compressive and tensile strains, so that the net strain across the whole structure is zero. It is also necessary to ensure that the thickness of any single layer does not exceed the critical thickness for the layer composition, which is easily satisfied for the Ge compositions used here ($\leqslant 35\%$). The structures were purchased from QinetiQ (formerly DERA) U.K., and grown by low-pressure chemical vapor deposition using an industry-standard Applied Materials Epi-Centura reactor. A number of samples have been investigated, and our three prototype sample structures are designated SQW2 (uncoupled quantum wells), QCL6, and QCL10 (quantum cascades), respectively. Layer thicknesses were measured by transmission electron microscopy (TEM), and the Ge mole fractions found by both energy-filtered TEM (EFTEM) and energy-dispersive x-ray (EDX) spectroscopy.[7] The schematic band diagrams and calculated subband edge energies for all three structures are shown in Fig. 1.

The uncoupled quantum well structure (SQW2) reported earlier[6] comprised ten modulation-doped $Si_{0.72}Ge_{0.28}$ quantum wells with Si barriers, and $Si_{0.78}Ge_{0.22}$ buffers, on a $Si_{0.78}Ge_{0.22}$ virtual substrate Above the strain-relaxation buffer, ten periods of 5 nm boron-doped $Si_{0.78}Ge_{0.22}$ ($N_A = 5\times10^{17}$ cm^{-3}), 2.8 nm i-$Si_{0.78}Ge_{0.22}$ spacer, 5.3 nm i-Si barrier, 12 nm i-$Si_{0.72}Ge_{0.28}$ quantum well, 5.3 nm i-Si barrier, 2.8 nm i-$Si_{0.78}Ge_{0.22}$ spacer, and 5 nm p-$Si_{0.78}Ge_{0.22}$ ($N_A = 5\times10^{17}$ cm^{-3}) was grown.

The QCL6 structure was composed of 20 periods of 6.6 nm $Si_{0.66}Ge_{0.34}$ quantum wells with 2.2 nm Si barriers on a $Si_{0.7}Ge_{0.3}$ virtual substrate. Unlike SQW2, it did not contain spacer regions. The quantum well layers were doped with a boron concentration of 7.5×10^{17} cm^{-3}. The bottom contact layer comprised 10 nm of 10^{18} cm^{-3} boron-doped $Si_{0.66}Ge_{0.34}$ while the top contact layer comprised 90 nm of 10^{19} cm^{-3} doped $Si_{0.66}Ge_{0.34}$ above 10 nm of 10^{18} cm^{-3} doped $Si_{0.66}Ge_{0.34}$.

More recently new prototype structures have been grown with a much larger number of total periods, which are thus better suited to laser cavity design. QCL10 is a 400-period structure with total active region thickness of $\sim$3.8 μm. The sample consisted of 400 4.4-nm-thick p-$Si_{0.75}Ge_{0.25}$ wells separated by 2.2 nm Si barriers. It was grown with intermittent doping: every 20th well in the stack, and the barriers immediately adjacent to those wells, were doped at 4×10^{18} cm^{-3} to ensure that a sufficient carrier density was present in these very long stacks for good current drive and optical power output. The doping densities used give an average sheet carrier density of 1.75×10^{11} cm^{-2} per well for this structure.

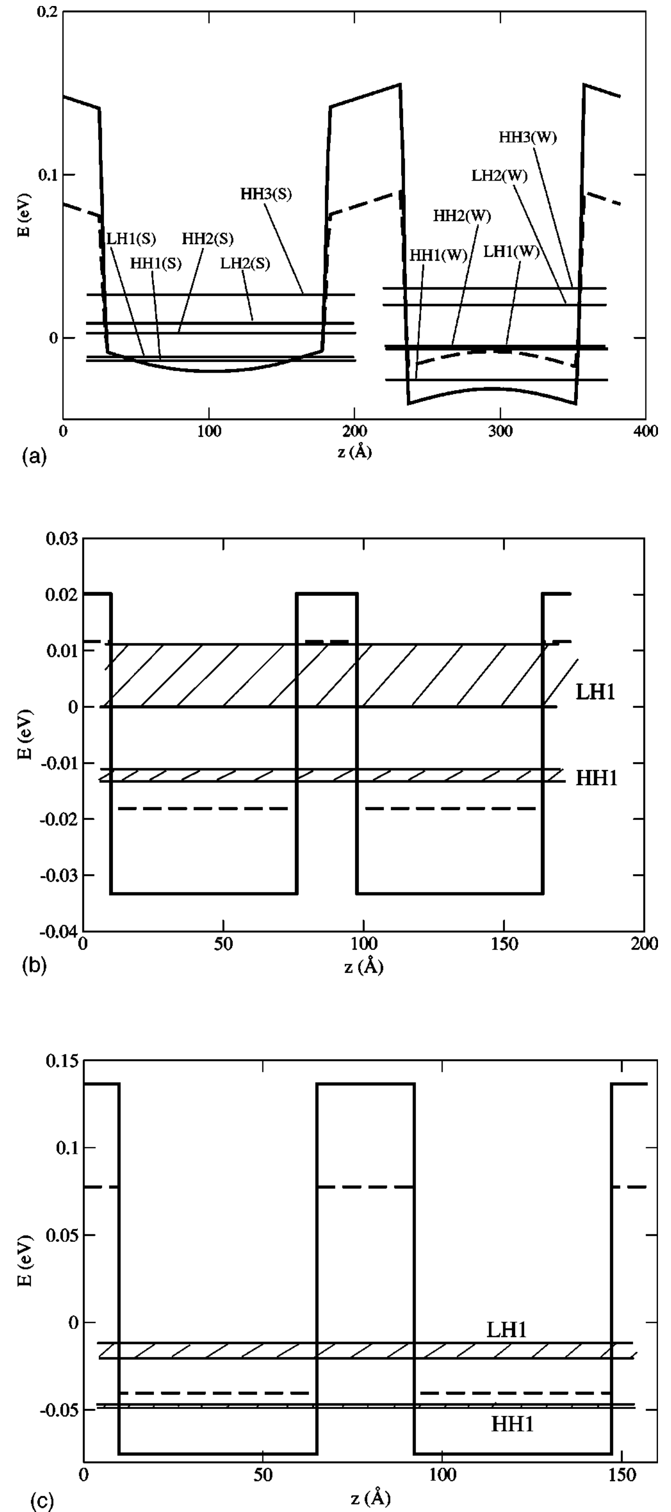

FIG. 1. Confinement potentials and calculated subband (or miniband) edge energies for the three samples studied: (a) SQW2, (b) QCL6, and (c) QCL10. The full and dashed curves show the confinement potentials for heavy and light holes respectively. In (a), one period of the ten-period structure is shown, and the suffixes (W) and (S) denote subbands localized in the quantum well and the adjacent spacer layer, respectively. In (b) and (c), two periods of the superlatticelike structures are shown; the shaded regions indicate the extent of the heavy and light hole minibands.

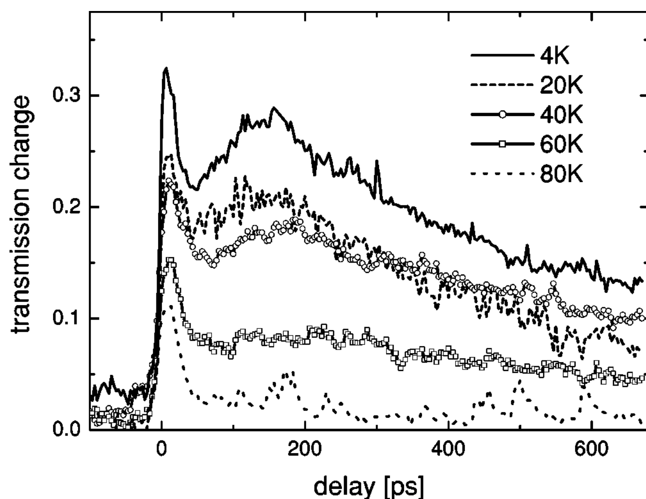

FIG. 2. Differential probe transmission vs optical delay for temperatures between 4 and 80 K at $\lambda=45$ μm for sample SQW2.

Electroluminescence spectra have been obtained for SQW2 and QCL6, and have confirmed the theoretical intrawell subband transition assignments.[8,9] In contrast with SQW2 and QCL6, QCL10 was designed to have predominantly diagonal (i.e., interwell) transitions under bias, and the design has been confirmed by electroluminescence spectroscopy.[10] The vertical (intrawell) transitions were not observed for QCL10 in electroluminescence, but we have measured them by both Fourier transform infrared (FTIR) absorption spectroscopy and by the FELIX pump-probe measurements described below.

Degenerate pump-probe measurements of nonradiative intersubband relaxation were made using the FELIX free-electron laser. A three-beam balanced pump-probe technique described earlier[11] was used in the far-infrared region of interest. The macropulse duration was 5 μs with 5 Hz repetition rate. The macropulse contained a train of micropulses of a minimum of 2 ps duration and 25 MHz repetition rate. A polarization rotator was used to change the polarization of the pump to be perpendicular to the probe, hence eliminating any so-called coherence artifact effect.[12] An analyzer was placed behind the sample to shield the detector from any scattered pump radiation.

III. EXPERIMENTAL RESULTS

A. SQW2

Pump-probe measurements were carried out on the uncoupled multiple-quantum-well structure SQW2 for a range of temperatures, with the pump beam tuned to the intersubband transition wavelength, obtained both from FTIR electroluminescence spectra and by maximizing the pump-probe transmission step. Degenerate pump-probe transmission spectra (showing the differential probe transmission as a function of delay behind the bleaching pump pulse) are shown in Fig. 2, for an excitation wavelength of 45 μm, in the temperature range 4–80 K. The incident beam angle for these measurements was 40°.

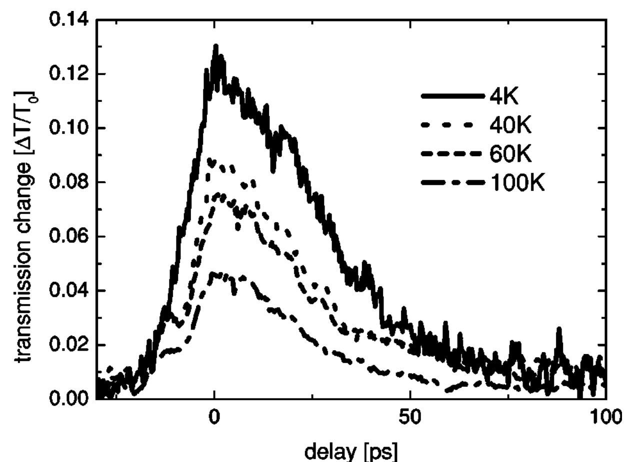

FIG. 3. Differential probe transmission vs optical delay for temperatures between 4 and 100 K, at $\lambda=95$ μm for sample QCL6.

Clearly, a dual-decay response is obtained for temperatures below 80 K. The sharp feature with an exponential decay time of 10–15 ps, which was present throughout the temperature range investigated, is associated with intersubband relaxation within the well. The subsequent, anomalous increase in transmission, followed by a slow decay, is associated with scattering into intermediate states confined in the spacer layers, as discussed previously.[6] The SQW2 structure has FIR absorbing states localized in the spacer layers, in the energy range between the HH1 and LH1 quantum well states, which are responsible for the dual-decay transmission response. Our measurements also indicate the striking result that the initial transmission decay is relatively independent of lattice temperature, in marked contrast with earlier measurements on the *n*-type GaAs/AlGaAs system.[13,14] The pump-probe experiments were performed on SQW2 for a range of pump wavelengths, confirming the resonance with the intersubband transition.

B. QCL6

The HH1-LH1 transition for QCL6 (which was predicted, and confirmed by electroluminescence spectroscopy,[10] to be at 95 μm) was investigated by pump-probe spectroscopy between 4 and 100 K as shown in Fig. 3. The incident beam was oriented normal to the sample surface. For this structure there are no spacer layers, and consequently we see only a single-decay response—i.e., the slow rise and decay at long times observed at low temperatures in SQW2 is absent here. Instead we see a transmission decay with an exponential decay time of $\sim$25 ps, which remains approximately constant throughout the range 4–100 K and is associated with intersubband relaxation within the well. Interesting results were obtained for this structure for a pump energy slightly off resonance (at 85 μm as shown in Fig. 4). It was possible to observe the pump-probe signal for even higher temperatures, up to room temperature, with an approximately constant scattering time of $\sim$20 ps. Figure 4 also shows a transient overshoot in the absorption, for temperatures of 60 K and below, with an extremely long recovery time.

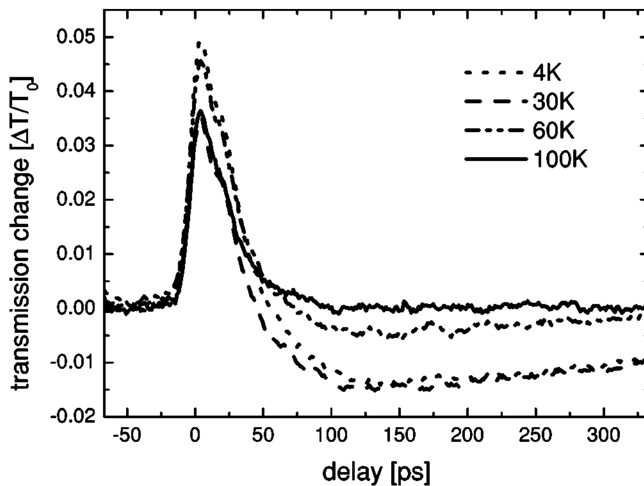

FIG. 4. Differential probe transmission vs optical delay for temperatures between 4 and 100 K at $\lambda=85$ μm for sample QCL6.

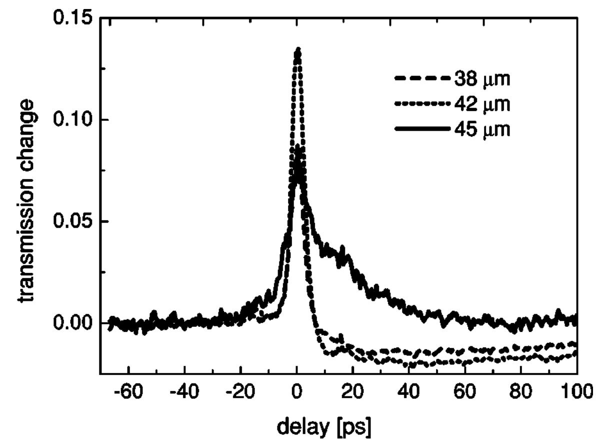

FIG. 5. Differential probe transmission vs optical delay at 4 K between 38 and 45 μm for sample QCL10.

C. QCL10

Results from pump-probe spectroscopy on the sample QCL10 are presented in Fig. 5. A lifetime of $\sim$2 ps was extracted for excitation at both 38 and 42 μm—considerably shorter than observed for both QCL6 and SQW2. These results were obtained using a surface-normal geometry as for QCL6. For excitation at 45 μm, a lifetime of $\sim$15 ps was observed. Figure 6 shows the transient absorption recovery at different temperatures, for a pump wavelength of 42 μm. The recovery lifetime appears to be approximately independent of temperature.

In summary, the three samples, all of which have an LH1-HH1 subband spacing smaller than the Ge-Ge phonon energy, have exhibited intersubband lifetimes ranging over approximately one order of magnitude. The lifetimes appear to be relatively insensitive to temperature in all three cases. In the following sections, our theoretical model and our theoretical analysis of these observations are presented.

IV. THEORETICAL MODEL

The hole subbands in each of the Si/SiGe heterostructures were calculated using the 6×6 $\mathbf{k}\cdot\mathbf{p}$ method with Foreman's boundary conditions,[15] which is sufficiently accurate for the range of energies involved in the structures considered.[16] The model fully accounts for the in-plane anisotropy and nonparabolicity of the subband dispersions, which occurs due to mixing of heavy, light, and spin-orbit split-off bulk states in the hole subbands. The subband energies and wave functions were calculated for a range of in-plane wave vectors, and were then used to evaluate hole scattering and intersubband absorption rates.

The calculation of optical intersubband absorption transitions was performed in the conventional manner, by evaluating the matrix elements of velocity (the commutator of the Hamiltonian and coordinate, with the position dependence of the Luttinger parameters taken into account) across the in-plane wave-vector space. Summation over in-plane wave vectors was then performed, while accounting for the actual subband dispersion, and a homogeneous linewidth of 4 meV (full width at half maximum) was assumed. This value is merely an estimate, but the precise value is not very important because our band structure calculations indicate that most of the total linewidth in the structures considered is due to the nonparallel nature of the subband dispersions.

The most important scattering processes in Si/SiGe heterostructures are deformation potential scattering (by both acoustic and optical modes) and alloy disorder scattering.[17] Optical deformation potential phonon scattering of holes in the SiGe quantum well layers is described by three distinct modes (corresponding to Ge-Ge, Ge-Si, and Si-Si interatomic vibrations), each having a weight proportional to the number of interatomic bonds in an alloy of a given composition.[18] Given the small LH1-HH1 energy spacing in all three structures considered here, only the Ge-Ge mode, with a phonon energy of 37 meV, is predicted to have any significant influence on the LH1-HH1 intersubband lifetime. Acoustic deformation potential phonon scattering, however, is always important in p-type Si/SiGe structures with small subband separations. In calculations of scattering rates both types of phonons were considered to be bulklike [any pho-

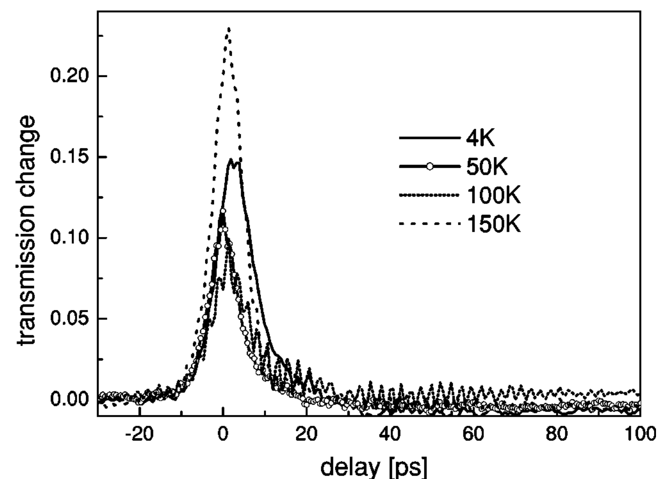

FIG. 6. Differential probe transmission vs optical delay at 42 μm between 4 and 150 K for sample QCL10.

non confinement effects in the nonpolar Si/SiGe system are expected to be relatively weak, compared to those predicted in polar heterostructures such as GaAs/AlAs (Refs. 19 and 20)]. Optical phonons were assumed to be nondispersive, and acoustic phonons were taken to have linear dispersion (the quasielastic approximation is not used). The tensorial rather than scalar form of hole-phonon interaction Hamiltonian was used[21,22] (in contrast to our previous study of one of the structures[6]). Due to the nature of the hole subband dispersions, the scattering rates were calculated using a fully numerical scheme, employing the linear tetrahedron method.[23]

For acoustic phonon scattering we have used the deformation potentials $a=2.1$ (2.0), $b=-1.5$ (−2.2), $d=-3.4$ (−4.4), all in units of eV, and for optical phonons $DK_{op} = 32.9\ (35.5) \times 10^8$ eV/cm for Si (Ge).[21] The deformation potentials, as well as the sound velocity and material density, in the alloy layers (which are the hole-confining layers, and therefore the most important for scattering in *p*-Si/SiGe heterostructures) were obtained by linear interpolation. The accuracy of this approximation is not known. For instance, in the calculation of hole subbands the Luttinger parameters for the alloy layers are calculated by a procedure which does not correspond to linear interpolation between the Luttinger parameters for Si and Ge.[24] The possible effects of uncertainties over the exact interpolation law are discussed further below.

Another important scattering mechanism in *p*-Si/SiGe is alloy disorder scattering, due to local composition fluctuations of the alloy.[25,26] This is characterized by a single parameter, the alloy scattering potential, which was set to 0.15 eV in this work. This choice is explained in the following section.

For small subband spacings, intersubband carrier-carrier scattering may also be important for hole relaxation. Calculation of the carrier-carrier scattering rates is much more complicated for holes than for electrons. The scattering matrix elements were calculated as in,[27,28] but accounting for the spinor structure of the hole subband wave functions, and for the anisotropy of the subband dispersions. The linear tetrahedron method was again used for integration since, contrary to the case of the one-band effective-mass approximation, no analytic solutions were attainable within this model. Furthermore, single-subband static screening, calculated with the hole wave functions at the zone center only, was employed. Although this approach is less accurate than dynamic screening,[29] the latter would be computationally too demanding for holes, and the method employed here is expected to produce reasonable accuracy (well within an order of magnitude) for the hole-hole scattering rates.

The calculation of hole relaxation dynamics in FELIX experiments was performed by finding the particle scattering rates, as well as hole energy relaxation rates, at a number of carrier and lattice temperatures. These data were then assembled in look-up tables, which were used for interpolation when simulating the dynamics of the system after initial bleaching by the FELIX pulse, in a similar manner as was employed in recent calculations of hole transport in biased quantum cascade structures.[30] As the system evolved, the current values of subband populations and hole temperatures were used to calculate the absorption and extract its characteristic relaxation time. One unknown quantity in these simulations is the initial hole temperature immediately after the FELIX pulse. This temperature is certainly higher than the heat-sink temperature, because carrier heating occurs due to intrasubband optical absorption, but it is difficult to determine the extent of this heating. A weak dependence of relaxation times on the lattice temperature, as found in all three structures, may be taken to mean that the initial carrier temperature is sufficiently large (e.g., over 200 K) that the initial carrier distributions are the same throughout the range of lattice temperatures used. However, relaxation calculated under such conditions is too fast to match any experiment, because of the onset of strong optical phonon scattering. Therefore, the initial hole temperature, immediately after the FELIX pump pulse, was set to be 50 K above the lattice temperature; deviations around this value were found to have little influence on the final results.

One often neglected point is that the quantity actually measured in pump-probe experiments is the relaxation of optical transmission, rather than of the subband populations. The difference between these two quantities arises from the dependence of the optical transition matrix elements on in-plane wave vector. Hence, this distinction can safely be neglected for *n*-type heterostructures, where the optical matrix element is approximately constant throughout the range of **k** space of interest, but should not be ignored for the case of *p*-type structures, as studied here, where the mixing of heavy, light, and spin-split-off valence states gives rise to significant variations in the matrix elements. We have carried out calculations of both population and absorption relaxation rates, under various levels of approximation: the difference between these models is highlighted below.

V. THEORETICAL RESULTS

A. QCL10

The QCL10 structure is a superlattice, with an HH1 miniband of approximately 1 meV width, and an LH1 miniband of approximately 5 meV width [refer to Fig. 1(c)]. Optical absorption is permitted from the bottom of the HH1 miniband to the bottom of the LH1 miniband; from the top of HH1 to the top of LH1, and between all intermediate HH1 and LH1 states of like symmetry. Given that states across the thin HH1 miniband are approximately equally populated, even at very low temperatures, the minibands add about 4 meV to the total linewidth for the HH1-LH1 transition. The FELIX experiments indicate that strong absorption was observed in the QCL10 structure at a wavelength of 38 μm, corresponding to a photon energy of 32.7 meV. To match this transition theoretically, we have to postulate a Ge mole fraction in the quantum wells of 31% (rather than the target 30%): this is quite likely given the epitaxy tolerances and the difficulties of performing accurate EFTEM or EDX composition measurements on very thin layers. Figure 7 shows the calculated LH1-HH1 relaxation times for QCL10 as a function of lattice temperature, assuming 31% Ge mole fraction in the quantum wells and using the measured layer thicknesses. Both the bare population relaxation times and the

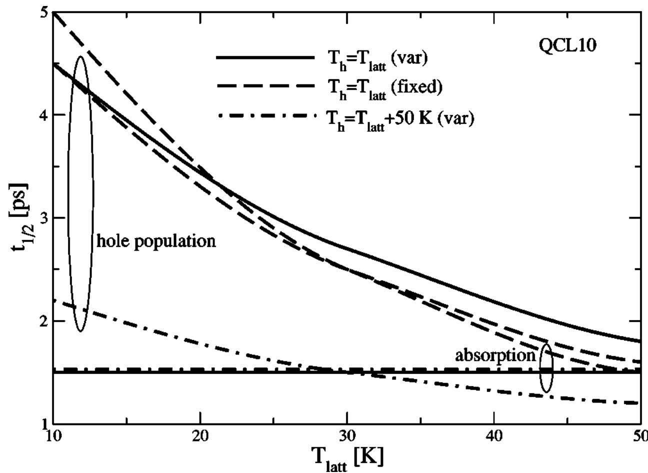

FIG. 7. Comparison of simulated transmission relaxation and hole population relaxation lifetimes for the QCL10 structure, as a function of lattice temperature (T_{latt}). The simulations were performed using the self-consistent energy balance method with the initial carrier temperature (T_h) set equal to T_{latt} (full curves), and with the initial T_h set 50 K above T_{latt} (dot-dashed curves). Simulations were also carried out without energy balance, keeping T_h fixed throughout each simulation (long-dashed curves).

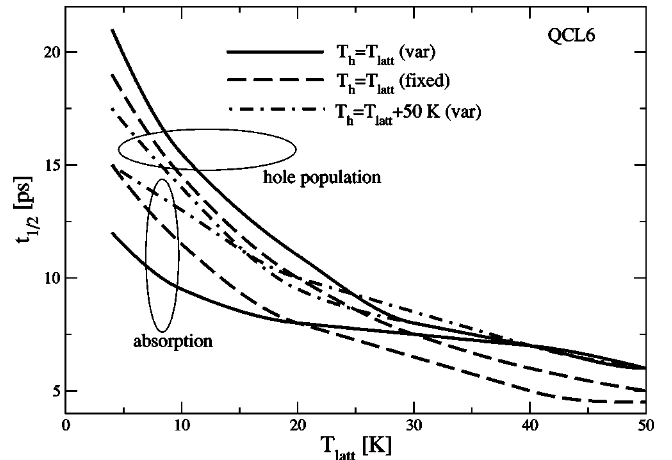

FIG. 8. Simulated transmission relaxation and hole population relaxation lifetimes for QCL6, as a function of lattice temperature (T_{latt}). Key as for Fig. 7.

optical transmission relaxation times are calculated, each under three different conditions: first, with the initial carrier temperature set equal to the lattice temperature, but allowed to vary during the transient simulation through the energy balance calculation;[31] second, with the carrier temperature tied to the lattice temperature throughout each transient simulation (no energy balance); and third, with the initial carrier temperature set 50 K above the lattice temperature, but allowed to vary with time as in the first case. As we have discussed above, it is the last of these cases, which allows for some initial heating of the carrier population by the pump pulse, that we believe to be the most realistic. When this scheme is applied to the simulation of optical absorption recovery (transmission decay), a lifetime of 1.5 ps is obtained—in excellent agreement with experiment—which stays remarkably constant throughout the temperature range shown. For this structure, the initial carrier heating appears to make little difference to the calculated lifetime; however, accounting for energy balance throughout each transient simulation is important; simulations in which the carrier temperature is kept constant lead to a large overestimation of the lifetime, especially at low temperatures. For QCL10, the population and transmission relaxation times are quite similar, provided the energy balance model is used with initial carrier heating. However, the population relaxation shows a stronger temperature dependence. This is expected: the relatively short LH1-HH1 lifetime at 38 μm (32.7 meV) in this structure, compared to the other two structures investigated, corresponds to the fact that the subband energy spacing in QCL10 was closest to the Ge-Ge phonon energy. Consequently, the Ge-Ge mode deformation potential optical phonon scattering is the dominant process. As the lattice temperature is increased, more optical phonon scattering occurs because a greater proportion of the LH1 carrier distribution is able to emit optical phonons. However, this temperature dependence is compensated for by the temperature-induced change in the probability of optical transitions which arises from the change in the **k**-space distribution of the LH1 carrier population.

The measured data also show a signal at 45 μm (27.6 meV), with a much longer relaxation time ($\sim$15 ps). While this shift in transition energy can be explained by either the miniband widths or the homogenous broadening, neither of these explains the increase in lifetime. On the other hand, a change in both lifetime and transition energy can be explained by a shift in the perpendicular (superlattice) and in-plane wave vectors at which the transitions occur. The lifetime is then expected to increase, since the transition energy is further from the Ge-Ge phonon energy. Simulations for the case of optical excitation at 45 μm gave a LH1 lifetime of 5 ps at a lattice temperature of 4 K—consistent with the experimental trend, but, quantitatively, a factor of 3 faster than the measured value.

The simulations were repeated with intersubband hole-hole scattering included, using the average sheet carrier density of 1.75×10^{11} cm^{-2} quoted above. The hole-hole scattering was found to make very little difference to the overall LH1-HH1 relaxation times in this structure.

B. QCL6

The QCL6 structure is also a narrow-band superlattice but, because of the smaller difference between the Ge mole fractions in the quantum wells and buffer, and consequent reduced strain in the quantum wells, compared to the case of QCL10, the HH1 and LH1 minibands are much closer together, with a calculated spacing of 13 meV [see Fig. 1(b)]. This corresponds very well to the experimentally determined intersubband absorption maximum at 95 μm. Since the subband spacing is much smaller than the Ge-Ge phonon energy, longer lifetimes are expected. Figure 8 shows the simulated lifetimes as a function of carrier temperature, calculated for both population and transmission relaxation, using the same models as discussed above for QCL10. The variable

carrier temperature model with initial heating gives a transmission decay lifetime of 15 ps at a lattice temperature of 4 K. At low temperatures, the population relaxation times are consistently longer than those for transmission relaxation. While transmission relaxation is clearly the appropriate quantity to model, in order to match the experimental data, the **k** dependence of the optical matrix elements involved in this calculation is very sensitive to the exact nature of the band structure, and therefore to the exact structural parameters of the sample. Indeed, while both QCL10 and SQW2 were of very high structural quality, with extremely planar layers, TEM images of QCL6 showed clear evidence of low-amplitude oscillations in the layers, due to residual strain, which results in a variation of layer thicknesses across the plane of the structure, and consequent variation of the precise details of band structure. Figure 8 thus implies that the lifetime for QCL6 lies approximately in the range 15–20 ps, which is in reasonable agreement with the measured value of ~25 ps, and confirms the observed trend of much longer lifetime for QCL6 than for QCL10.

As the lattice temperature is increased, the simulations all predict a decrease in lifetime (whichever model is used), which does not seem apparent in the measurements. The simulations show that, because the LH1-HH1 subband separation is so small compared to the Ge-Ge phonon energy, optical phonon scattering is negligible throughout the temperature range considered. The lifetime is therefore dominated by acoustic phonon scattering and alloy disorder scattering. The temperature dependence in the simulations arises directly from the increase in acoustic phonon population with lattice temperature—so the difference between theory and experiment cannot be explained by any uncertainties over the carrier temperatures (and the extent of any localized lattice heating produced by the FELIX beam in these experiments is estimated to be insignificant). On the other hand, the alloy disorder scattering rate is approximately constant with temperature (it actually decreases slightly as the lattice temperature increases) so the experimental results imply that the acoustic phonon scattering is weaker than in our simulations, such that alloy scattering dominates. This point is discussed further below.

We also considered the effect of intersubband hole-hole scattering in this sample. There are a number of uncertainties here; both in the carrier density in the quantum wells at any given temperature and in the calculation of the hole-hole scattering rate itself. Although only the quantum well layers are intentionally doped, diffusion of boron into the silicon barriers occurs during growth. Based on typical secondary ion mass spectrometry data for SiGe heterostructures,[32] we may assume that the boron concentration falls at a rate of approximately 1 decade every 4 nm into the silicon barrier. This gives an average doping density in the barriers of 2.8×10^{17} cm^{-3} (equivalent sheet density of 6×10^{10} cm^{-2}), and all these dopants are expected to release carriers into the adjacent quantum well layers, even at low temperatures. On the other hand, the dopants in the quantum well layer will only be partially ionized: at 4 K, the ionization fraction is less than 0.1%, and the carrier density is due solely to boron diffusion (giving $p=6\times10^{10}$ cm^{-2} per well). At the upper limit of the temperature range used, $T=100$ K, the ionization fraction is 30% (accounting for the screening-induced reduction of the ionisation energy,[33] but neglecting any quantum confinement effects on the dopants), giving a total carrier density of $\sim1.9\times10^{11}$ cm^{-2} per well. For these carrier densities, our calculated intersubband hole-hole scattering lifetimes are 12 and 8 ps, respectively. These clearly lead to overall intersubband lifetimes that are less than the measured values; however, they already indicate that intersubband carrier-carrier scattering is not an exceptionally fast process in this structure. As mentioned above, we have used a relatively simple screening model for the hole-hole scattering calculations, and this, in conjunction with the uncertainty over the exact carrier density, is probably sufficient to account for the fact that intersubband hole-hole scattering was not found to be significant in the experimental measurements.

The transmission response for an excitation wavelength of 85 μm was also investigated. The detuning from 95 to 85 μm represents a change in the pump photon energy of only ~1.5 meV, and this produces very little difference in the simulated response. Our model does not include the details of *intrasubband* carrier relaxation (the distribution functions are assumed to have a Fermi-Dirac form, for the calculated carrier temperature), and it is possible that the observed absorption overshoot and subsequent decay (Fig. 4) may be due to intrasubband hole cooling from stronger to weaker far-infrared absorbing states. However, even assuming that intrasubband carrier-carrier scattering is very weak, following the discussion above, the recovery time is still slower than that resulting from intrasubband acoustic phonon scattering, so there is little evidence to support this explanation.

C. SQW2

The calculated zone-center LH1-HH1 subband spacing in this structure was 24 meV, with the HH2 subband located just 2 meV below LH1 [see Fig. 1(a)]. While the LH1-HH1 spacing is slightly smaller than the phonon energy for the 45 μm excitation used experimentally, optical absorption is clearly possible given the assumed 4 meV homogeneous linewidth. Using this linewidth, optical absorption from HH1 to HH2 would not be possible at the zone center, although it would be possible for some nonzero values of in-plane wave vector, due to the distorted nature of the subband dispersion curves. Thus, although the 40° beam angle allows coupling to both HH1-LH1 and HH1-HH2 optical transitions, the observed response is expected to represent primarily carrier relaxation from LH1. In fact, the calculations show that, for cases such as this, where the LH1 and HH2 subbands are in close proximity, and hence strongly mixed, the intersubband lifetimes for each are very similar. Using the tensorial phonon scattering Hamiltonians, the simulated lifetimes were ~14–18 ps in the temperature range 4–60 K. This range of values, and the relatively weak temperature dependence, are both in good agreement with the experimental observations. Inclusion of hole-hole scattering in the simulations had very little effect on these lifetimes.

VI. DISCUSSION

To summarize from the above results, we obtain good agreement between theory and experiment for the intersub-

band transition energies and the low-temperature intersubband lifetimes for all three structures: QCL10 (short, ~2 ps lifetimes), QCL6 (long, ~20–25 ps lifetimes), and SQW2 (~10–15 ps lifetimes). The weak temperature dependence of lifetime observed in all three structures was reproduced theoretically for QCL10 and SQW2, but the simulations for QCL6 showed a somewhat stronger temperature variation. As mentioned above, this latter observation implies that the acoustic phonon scattering rate might be slower than that used in our simulations.

There are no fitting parameters in the phonon scattering rates, but it is difficult to obtain precise values for the various valence band deformation potentials. For acoustic phonon scattering, we have used values of the deformation potentials a, b, and d,[21] which were originally given by Wiley.[34] In his paper, Wiley indicated an uncertainty of approximately 25% in the values of b and d. An alternative set of parameters (for silicon) has been proposed by Fischetti *et al.*,[22] which were obtained by fitting the calculated low-field mobility for bulk silicon to experimental data. However, these values result in shorter intersubband lifetimes than reported above. While fitting to low-field mobility is a valuable exercise, it still does not enable evaluation of a, b, or d independently. Such independent determination is not important for bulk mobility calculations, as can be seen from the fact that results obtained using the tensor hole-phonon scattering Hamiltonian can be reproduced using a directionally averaged scalar Hamiltonian.[22] However, for intersubband scattering in quantum well systems, the direction averaging does not apply, and the phonon scattering rates for the LH1-HH1 transition calculated using the exact tensor Hamiltonian are larger than those obtained with an effective scalar deformation potential calculated using the same values of a, b, and d. Given that the bulk mobility experiments can be fitted by an effective scalar deformation potential of the form[22,34]

$$\Xi_{eff}^2 = a^2 + \frac{c_l}{c_t}\left(b^2 + \frac{d^2}{2}\right), \tag{1}$$

where c_l and c_t are the effective longitudinal and transverse crystal elastic constants, we tried varying the values of the deformation potentials b and d, while keeping the factor $(b^2+d^2/2)$ constant. However, this yielded very little difference in the calculated acoustic phonon scattering rates.

We also investigated the possible errors introduced by interpolation of the various scattering parameters. As mentioned above, each individual scattering parameter has been interpolated linearly between the published values for Si and Ge. This results in a hybrid interpolation curve for the scattering rates which is not exactly linear, but is reasonably close to a linear relationship. However, for Si-rich alloy layers ($x<0.5$), as is the case for all three structures considered here, the errors introduced by interpolation are unlikely to be greater than the difference between the calculated rates and those for the case of pure silicon, and in the case of QCL6 ($Si_{0.66}Ge_{0.34}$ quantum wells) this difference is less than 10%.

In order to eliminate the temperature dependence from the simulated LH1 lifetimes for QCL6, we found that it was necessary to reduce the acoustic phonon scattering rate by a factor of more than 4, compared to the values obtained using the above model. This could be achieved, for example, by reducing each of the acoustic deformation potentials by a factor of 2, but such an adjustment would not be consistent with the bulk mobility experiments.

Of course, both the value and temperature dependence of the lifetimes in structures with small subband spacings are also influenced by alloy disorder scattering: stronger alloy scattering will give a weaker temperature dependence, but at the expense of a shorter overall lifetime. The alloy scattering potential is perhaps the most uncertain of all the scattering parameters in the model, and a range of values has been reported in the literature. We found that the best matches to the measured lifetimes for both QCL6 and SQW2 were obtained by using a value of 0.15 eV for the scattering potential (normalized to the primitive cell volume), which lies at the lower end of the reported range. (While we had used a larger value in our previously reported calculations for SQW2,[6] this was used in conjunction with use of the approximate scalar Hamiltonian for phonon scattering, which gave slower scattering rates than the more accurate tensor Hamiltonian used here.)

The experimentally observed trend invites a relatively simple interpretation: that the LH1-HH1 lifetime increases progressively as the subband spacing is reduced because the optical transition energy is shifted further away from the Ge-Ge phonon energy. While this phenomenon certainly occurs, the theory indicates that there are also more subtle changes taking place. There is a large difference in lifetime between QCL10 and SQW2, even though the absorption energy changes by only ~5 meV (in comparison, the absorption energy in QCL6 is 20 meV different from that in QCL10). The calculations indicate that this change in lifetimes is also due to the different contributions of light-heavy hole mixing in the two structures. In QCL10, the HH2 subband is well separated from LH1, and therefore the LH1 subband experiences little mixing. On the other hand, in SQW2, the HH2 and LH1 subbands lie within 2 meV of each other, and so the light-heavy hole mixing is much stronger. In the tensor Hamiltonian formulation, phonon scattering between light and heavy hole states is stronger than that between two heavy hole states, for the same energy spacing. Thus, strong mixing of heavy hole character into the light hole subband will decrease the overall scattering rate.

Finally, we should mention that we also measured and calculated the HH2 intersubband lifetime for the QCL10 structure. The HH2 subband (which, like the other subbands in this superlattice structure, is actually a narrow miniband) lies approximately 70 meV above the HH1 miniband. The calculated lifetime at 4 K was less than 1 ps: pump-probe measurements at this temperature, for a pump wavelength of 17 μm (73 meV) gave a pulse-width-limited response—i.e., the measured lifetime was less than 2 ps (Fig. 9). We mention this to clarify that shorter lifetimes are expected for higher-lying subbands, compared to those discussed above, since all the principal phonon modes in the Si/SiGe system (in particular, the Si-Si mode at ~64 meV) can contribute to intersubband scattering.

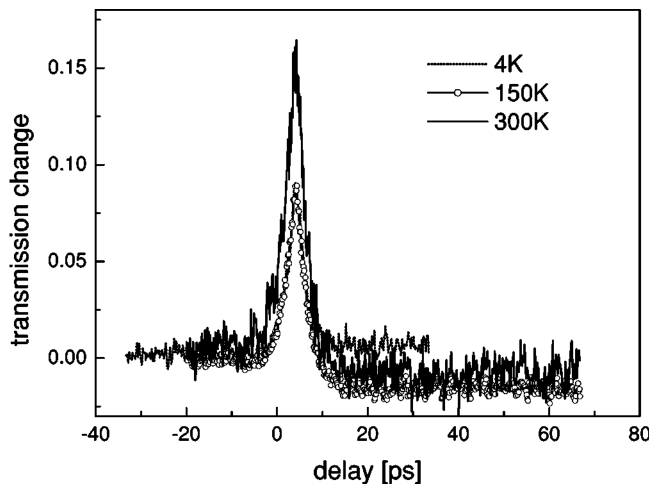

FIG. 9. Differential probe transmission vs optical delay at 17 μm, for temperatures from 4 to 300 K, for sample QCL10.

VII. CONCLUSIONS

Intersubband pump-probe spectroscopy has been carried out on three different *p*-Si/SiGe heterostructures using the FELIX free-electron laser, in order to measure the intersubband lifetime for the LH1-HH1 transition. In all cases, the LH1-HH1 subband spacing was less than the smallest optical phonon energy in the structure—that of the 37 meV Ge-Ge phonon mode. The measured lifetimes in the three structures ranged from 2 to 25 ps, with the lifetime increasing as the LH1-HH1 spacing was reduced. In all cases, the temperature dependence of the lifetime was found to be very weak, with little variation observed in the range 4–100 K, and in one measurement, throughout the range 4–300 K. A dual-decay response was found only in the case of the uncoupled multiple-quantum-well structure SQW2, and not in the case of the superlattice structures QCL6 and QCL10, confirming our hypothesis that the dual-decay response arose from scattering into intermediate states confined in the spacer layers between the wells of the SQW2 sample.

Simulations of the intersubband carrier dynamics in all three structures were carried out using six-band $\mathbf{k}\cdot\mathbf{p}$ calculations of the hole subbands and wave functions, together with calculations of phonon, alloy disorder, and hole-hole scattering, which were incorporated into a time-domain rate equation scheme. Good agreement between theory and experiment for the intersubband transition energies and intersubband lifetimes was obtained for all three structures, including quantum cascade structures with different Ge mole fractions, and a significantly different uncoupled quantum well structure. LH1 lifetimes ranging over an order of magnitude were reproduced using the same theoretical model in all cases. The simulations indicated that the increase in lifetime with reduced subband spacing was due primarily to the reduced contribution of Ge-Ge mode optical phonon scattering (which was found to be dominant in QCL10, but negligible in the case of QCL6) but showed that heavy-light hole mixing also played an important role in determining the lifetimes for a given subband separation. The theoretical model also highlighted the difference between the measured lifetimes for transmission relaxation in a pump-probe experiment and the actual intersubband population relaxation: this difference is a consequence of the variation of the optical matrix element with in-plane wave vector, and therefore is peculiar to *p*-type heterostructures.

The results highlight two main points relevant to the design of *p*-Si/SiGe quantum cascade lasers: first, that long intersubband lifetimes can be achieved (up to 25 ps), representing effective suppression of nonradiative processes by choosing subband spacings smaller than the optical phonon energies in the structure, and second, that *p*-Si/SiGe offers considerable scope for "lifetime engineering"—with observed variations of over an order of magnitude in lifetime—which will aid the design of structures having usable population inversions between subbands.

ACKNOWLEDGMENTS

The Si/SiGe quantum cascade program is funded by DARPA on USAF Contract No. F-19628-99-C-0074, by the EU on Contract No. IST-2001-38035"SHINE," and by EPSRC Grant No. GR/S27528. We are grateful for support for the U.K. program at FELIX from EPSRC (U.K.), and for the skillful assistance of Dr. A. F. G. van der Meer. We thank Dr. R. A. Soref, Hanscom AFB, Dr. J. Zhang, Imperial College, and Dr. D. J. Robbins, CENAMPS, for useful discussions.

---

*Email address: r.w.kelsall@leeds.ac.uk

[1] C. Gmachl, F. Capasso, D. L. Sivco, and A. Y. Cho, Rep. Prog. Phys. **64**, 1533 (2001).

[2] R. W. Kelsall and R. A. Soref, in *Terahertz Sensing Technology*, edited by D. L. Woolard, W. R. Loerop, and M. S. Shur (World Scientific, Singapore, 2003).

[3] R. W. Kelsall, Z. Ikonic, P. Harrison, S. A. Lynch, R. Bates, D. J. Paul, D. J. Norris, S. L. Liew, A. G. Cullis, D. J. Robbins, P. Murzyn, C. R. Pidgeon, D. D. Arnone, and R. A. Soref, in *Towards the First Silicon Laser*, edited by L. Pavesi, S. Gaponenko, and L. Dal Negro, NATO Science Series (Kluwer, Dordecht, 2003).

[4] R. Kohler, A. Tredicucci, F. Beltram, H. Beere, E. Linfield, G. Davies, D. Ritchie, R. C. Iotti, and F. Rossi, Nature (London) **417**, 156 (2002).

[5] M. Rochat, L. Ajili, H. Willenerg, J. Faist, H. Beere, E. Linfield, G. Davies, and D. Ritchie, Appl. Phys. Lett. **89**, 1381 (2002).

[6] P. Murzyn, C. R. Pidgeon, J.-P. R. Wells, I. V. Bradley, Z. Ikonic, R. W. Kelsall, P. Harrison, S. A. Lynch, D. J. Paul, D. D. Arnone, D. J. Robbins, D. Norris, and A. G. Cullis, Appl. Phys. Lett. **80**, 1456 (2002).

[7] S. L. Liew, D. J. Norris, A. G. Cullis, R. W. Kelsall, P. Harrison,

Z. Ikonic, D. J. Paul, S. A. Lynch, R. Bates, and D. D. Arnone, *Microscopy of Semiconducting Materials 2003*, IOP Conf. Proc. No. 180 (Institute Of Physics, Bristol, 2003), pp. 155–158.

[8] S. A. Lynch, S. S. Dhillon, R. Bates, D. J. Paul, D. D. Arnone, D. J. Robbins, Z. Ikonic, R. W. Kelsall, P. Harrison, D. J. Norris, A. G. Cullis, C. R. Pidgeon, P. Murzyn, and A. Loudon, J. Mater. Sci. **B89**, 12 (2002).

[9] S. A. Lynch, R. Bates, D. J. Paul, D. J. Norris, A. G. Cullis, Z. Ikonic, R. W. Kelsall, P. Harrison, D. D. Arnone, and C. R. Pidgeon, Appl. Phys. Lett. **81**, 1543 (2002).

[10] R. Bates, S. A. Lynch, D. J. Paul, Z. Ikonic, R. W. Kelsall, P. Harrison, S. L. Liew, D. J. Norris, A. G. Cullis, W. R. Tribe, and D. D. Arnone, Appl. Phys. Lett. **83**, 4092 (2003).

[11] P. C. Findlay, C. R. Pidgeon, R. Kotitschke, A. Hollingworth, B. N. Murdin, C. J. G. Langerak, A. F. G. vand der Meer, C. M. Ciesla, J. Oswald, A. Homer, G. Springholz, and G. Bauer, Phys. Rev. B **58**, 12 908 (1998).

[12] S. Hughes, C. M. Ciesla, B. Murdin, C. R. Pidgeon, D. Jaroszynski, and R. Prazeres, J. Appl. Phys. **78**, 3371 (1995).

[13] B. N. Murdin, W. Heiss, C. J. G. M. Langerak, S. C. Lee, I. Galbraith, G. Strasser, E. Gornik, M. Helm, and C. R. Pidgeon, Phys. Rev. B **55**, 5171 (1997).

[14] C. D. Bezant, M. M. Chamberlain, H. P. M. Pellemans, B. N. Murdin, W. Batty, and M. Henini, Semicond. Sci. Technol. **14**, L25 (1999).

[15] B. A. Foreman, Phys. Rev. B **48**, 4964 (1993).

[16] Z. Ikonic, P. Harrison, and R. W. Kelsall, Phys. Rev. B **64**, 125308 (2001).

[17] Z. Ikonic, P. Harrison, and R. W. Kelsall, Phys. Rev. B **64**, 245311 (2001).

[18] K. Bhaumik, B. K. Ridley, and Y. Shacham-Diamand, J. Appl. Phys. **74**, 5546 (1993).

[19] W. Jiang and J. P. Leburton, J. Appl. Phys. **74**, 1652 (1993).

[20] V. M. Menon, W. D. Goodhue, A. S. Karakashian, and L. R. Ram-Mohan, J. Appl. Phys. **88**, 5262 (2000).

[21] J. M. Hinckley and J. Singh, J. Appl. Phys. **76**, 4192 (1994).

[22] M. V. Fischetti, Z. Ren, P. M. Solomon, M. Yang, and K. Rim, J. Appl. Phys. **94**, 1079 (2003).

[23] Z. Ikonic, R. W. Kelsall, and P. Harrison, Phys. Rev. B **69**, 235308 (2004).

[24] C. M. deSterke, Phys. Rev. B **36**, 6574 (1987).

[25] K. Yeom, J. M. Hinckley, and J. Singh, J. Appl. Phys. **80**, 6773 (1996).

[26] M. J. Kearney and A. I. Horrell, Semicond. Sci. Technol. **13**, 174 (1998).

[27] J. H. Smet, C. G. Fonstad, and Q. Hu, J. Appl. Phys. **79**, 9305 (1996).

[28] P. Kinsler, P. Harrison, and R. W. Kelsall, Phys. Rev. B **58**, 4771 (1998).

[29] S. C. Lee and I. Galbraith, Phys. Rev. B **59**, 15 796 (1999).

[30] Z. Ikonic, P. Harrison, and R. W. Kelsall, Physica E (Amsterdam) **21**, 907 (2004).

[31] Z. Ikonic, P. Harrison, and R. W. Kelsall, J. Comput. Electron. **2**, 353 (2003).

[32] J. Zhang (private communication).

[33] J. L. Pearson and J. Bardeen, Phys. Rev. **75**, 865 (1949).

[34] J. D. Wiley, Solid State Commun. **8**, 1865 (1970).